Article:
De Marco, M, Menzel, R, Bawaked, SM et al. (2017) Hybrid effects in graphene oxide/carbon nanotube-supported Layered Double Hydroxides: Enhancing the CO_2 sorption properties. Carbon, 123. pp. 616-627. ISSN: 0008-6223

https://doi.org/10.1016/j.carbon.2017.07.094

Accepted Manuscript

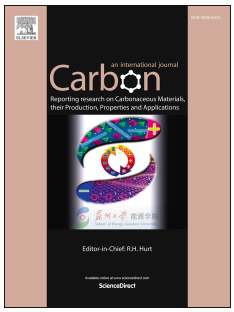

Hybrid effects in graphene oxide/carbon nanotube-supported Layered Double Hydroxides: Enhancing the CO_2 sorption properties

Martina De Marco, Robert Menzel, Salem M. Bawaked, Mohamed Mokhtar, Abdullah Y. Obaid, Sulaiman N. Basahel, Milo S.P. Shaffer

PII: S0008-6223(17)30777-7

DOI: 10.1016/j.carbon.2017.07.094

Reference: CARBON 12260

To appear in: *Carbon*

Received Date: 17 April 2017

Revised Date: 29 July 2017

Accepted Date: 31 July 2017

Please cite this article as: M. De Marco, R. Menzel, S.M. Bawaked, M. Mokhtar, A.Y. Obaid, S.N. Basahel, M.S.P. Shaffer, Hybrid effects in graphene oxide/carbon nanotube-supported Layered Double Hydroxides: Enhancing the CO_2 sorption properties, *Carbon* (2017), doi: 10.1016/j.carbon.2017.07.094.

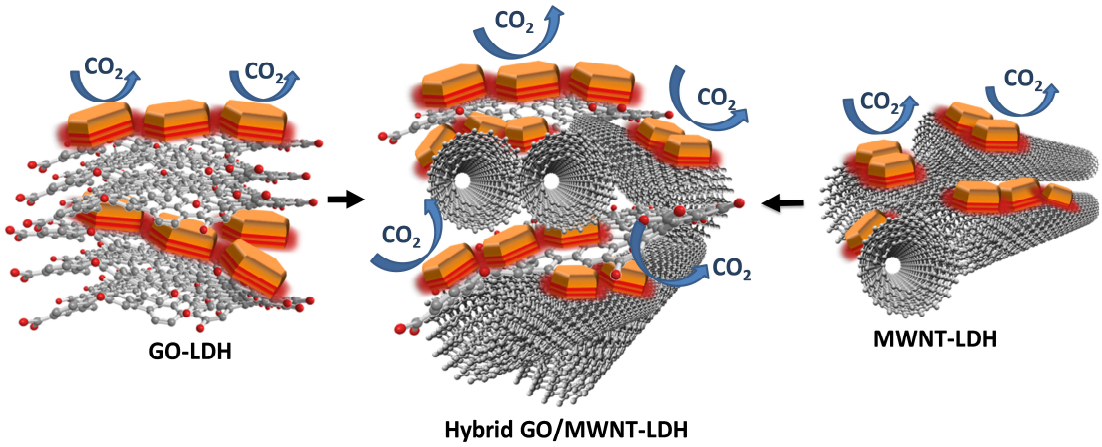

Hybrid Effects in Graphene Oxide/Carbon Nanotube-Supported Layered Double Hydroxides: Enhancing the CO_2 Sorption Properties

Martina De Marco,[a] Robert Menzel,[a,b] Salem M. Bawaked,[c,d] Mohamed Mokhtar,[c,d] Abdullah Y. Obaid,[c,d] Sulaiman N. Basahel,[c,d] and Milo S. P. Shaffer [a *]

a. Department of Chemistry Imperial College London, South Kensington Campus, London SW7 2AX, U.K.
b. School of Chemistry, University of Leeds, Leeds, LS2 9TJ, UK
c. Department of Chemistry, Faculty of Science, King Abdulaziz University, Jeddah, Saudi Arabia.
d. Surface Chemistry and Catalytic Studies Group, King Abdulaziz University, Jeddah, Saudi Arabia.

Graphene oxide (GO) and multi-walled carbon nanotubes (MWCNT) have been previously used independently as active supports for Layered Double Hydroxides (LDH), and found to enhance the intrinsic CO_2 sorption capacity of the adsorbents. However, the long-term stability of the materials subjected to temperature-swing adsorption (TSA) cycles still requires improvement. In this contribution, GO and MWCNT are hybridized to produce mixed substrates with improved surface area and compatibility for the deposition of LDH platelets, compared to either phase alone. The incorporation of a robust and thoroughly hybridized carbon network considerably enhances the thermal stability of activated, promoted LDH over twenty cycles of gas adsorption-desorption (96% of retention of the initial sorption capacity at the 20th cycle), dramatically reducing the sintering previously observed when either GO or MWCNT were added separately. Detailed characterization of the morphology of the supported LDH, at several stages of the multicycle adsorption process, shows that the initial morphology of the adsorbents is more strongly retained when supported on the robust hybrid GO/MWCNT network; the CO_2 adsorption performance correlates closely with the specific surface area of the adsorbents, with both maximized at small loadings of a 1:1 ratio of GO:MWCNT substrate.

1. Introduction

Layered double hydroxides (LDH) are lamellar hydroxides of the family of hydrotalcites (HT), with general formula $(M^{2+}_{1-x}M^{3+}_{x}(OH)_2)^{x+}(A^{m-}_{x/m}\,nH_2O)^{x-}$, where M^{2+}, M^{3+} and A^{m-} most commonly represent Mg^{2+}, Al^{3+} and CO_3^{2-} respectively (Brucite), although many other compositions occur.[1] Brucite-like sheets of octahedrally-coordinated divalent cations (typically Mg^{2+}) undergo a partial substitution by the trivalent cations (typically Al^{3+}), generating a net positive charge that is balanced by the intercalated anions (typically CO_3^{2-}). The intrinsic properties of these compounds have stimulated

* corresponding author. Tel: +44 20 7594 5825. E-mail: m.shaffer@imperial.ac.uk.

interest in a diverse range of applications, including as catalysts (aldol condensation, epoxidations, alkene isomerisations reactions, *etc.*),[2] biomedical vectors,[3, 4] flame retardants,[5] adsorbents[6] and nanocomposite reinforcements.[7] In particular, the Mg/Al LDH family (with Mg:Al ratios of 2 and 3) has been extensively studied in the past years, and recognised as an excellent composition for CO_2 adsorption applications.[8] The gas adsorption properties are manifested after thermal treatment of the material, that evolves into an active mixed metal oxide (MMO) form with finer particle size and increased surface area compared to the original structure. The associated progressive dehydroxylation and decarbonation of the structure generates the basic sites responsible for the subsquent (acid-base type) interaction with the CO_2 molecules.[9] Compared to known low temperature CO_2 solid adsorbents (such as zeolites, activated carbons, and metal organic frameworks), thermally-activated LDH typically manifest a lower intrinsic specific CO_2 adsorption capacity, but can operate at higher temperatures.[10] On the other hand, they manifest faster adsorption kinetics and much better regenerability than other high temperture solid adsorbents (such as lithium zirconates and calcium oxides).[11] LDH are frequently supported on high surface area substrates in order to improve adsorption capacity and stability over prolonged use, aspects that still hamper practical industrial implementation.

Amongst the materials tested as supports in these applications, carbon nanostructures (CN), including carbon nanofibers (CNF),[12] multi walled-carbon nanotubes (MWCNT)[13, 14] and graphene oxide (GO),[15, 16] have shown the most promise, particularly compared to more conventional systems based on alumina or zeolites.[17, 18] These carbon allotropes exhibit an intriguing combination of mechanical,[19, 20] thermal,[21] and electrical[22] characteristics, as well as high aspect ratios and surface areas,[23] which make them suitable for preparing robust, porous and high surface supporting networks.[24] Activated carbons are a possible alternative high surface area substrate,[25, 26] but tend to have relatively inaccessible slit micropores that are readily blocked by LDH deposition.[27] The use of LDH/ nanocarbons composites has been considered for a wide range of applications,[28, 29] but here we focus on CO_2 sorption. Mg/Al LDH platelets loaded dilutely on CNF (up to 90 wt% carbon), were reported to manifest an order of magnitude increase in the CO_2 adsorption capacity compared to the unsupported counterparts.[12] Oxidized MWCNT were subsequently adopted as supports,[13] where the acidic surface was used to drive nucleation of the positively-charged LDH platelets through electrostatic interactions; once activated, these MWCNT-LDH exhibited significant enhancement of the first-contact gas adsorption capacity compared to the unsupported material. In addition, an improvement in the multicycle stability was observed over twenty continuous cycles of gas adsorption-desorption.[13] The improvements were

attributed to a reduction in the LDH particle size and an associated increase in the basic site concentration available for gas adsorption.[30] Subsequently, 2 - 30 wt% of a GO substrate was found to be even more effective than the other CN for improving the CO_2 adsorption performance of LDH;[16, 31] the improvement was attributed to the two-dimensional geometric compatibility of the GO nanosheets with LDH platelets. Small loadings of GO were found to be most promising, with benefits plateauing at higher concentrations due to apparent restacking of the carbon sheets. However, it is not clear whether the GO only promotes multicycle stability or also first-contact adsorption capacity.[16, 32] In addition to the use of a support, the CO_2 adsorption capacity of LDH can be improved by doping with alkali metals.[33, 34] The benefits of alkali metal promotion have been confirmed with both CNF-LDH[34] and GO-LDH[16] materials; in general, residual sodium from the LDH synthesis may remain in the LDH, resulting in a significant enhancement of the first-contact adsorption capacity.[16] Whilst the literature identifies consistent trends for the adsorption capacity of CN-LDH hybrids, the absolute capacities vary due to the specific adsorption conditions adopted, including adsorption temperature and pressure, presence of water, concentration of carbon support and degree of doping.

Overall, the multicycle stability of CN-LDH still has considerable scope for improvement; for instance, for the best materials reported so far (GO-LDH), the loss of CO_2 adsorption performance over 20 cycles of gas adsorption-desorption under dry conditions remained a significant 15 - 40% (though improved compared to the 50 - 60% loss for pure LDH).[16, 31] Despite their promise, neither MWCNT nor GO are ideal supports: MWCNT, though offering a mechanically strong network for LDH deposition, require higher loadings to match the performance improvement provided by GO, as the surface area is not as intrinsically high, and the geometry less well matched. Increased CN loading negatively impacts the overall cost and weight of the final sorbent. On the other hand, GO alone has poor network forming ability, limiting benefits even at modest carbon loadings due to restacking of the sheets.

Recently, hybrid GO/MWCNT systems have been reported to exhibit interesting synergistic effects in certain applications.[35-38] Most studies focus on improvements in the properties of electrochemical double layer (EDLC) supercapacitors using hybrid GO/CNT electrodes, compared to carbon nanotubes (CNTs) and GO used independently.[39, 40] Hybrid GO/CNT electrodes have also been found to offer superior drug and gas sensing performance.[41] GO/CNT hybrids are compatible chemically due to the π-π attractions between basal planes and the hydrogen bonding between acidic functional groups.[40] Geometrically, CNTs act as spacers between the graphene sheets, preventing restacking and agglomeration. The enhanced overall surface area of the structure facilitates the access of electrolytes (for electrochemical

applications) and may improve the transport of gases (in adsorption applications). GO can help to form intimately mixed hybrid structures by acting as a dispersing agent for unoxidized-SWCNT[42] or MWCNT[43].

In principle, hybridized GO/MWCNT constructs are appealing as LDH supports, but have not yet been thoroughly studied because of the complexity of the resulting three-phase mixture (GO/MWCNT/LDH), although some recent reports have indicated promising potential for the use of hybrid graphene/nanotube systems to support LDH for catalytic (NiFe-LDHs)[44] or electrochemical (NiAl-LDH)[45] applications. Our aim was to explore GO/MWCNT hybrids in more detail, and specifically in the context of CO_2 sorption, in order to overcome the limitations identified for LDH supported on either GO or oxidized MWCNT, separately. We promoted the material with a small amount (5 wt%) of potassium to improve the absolute performance and avoid variations due to low loadings of adventitious alkali metal. The materials were tested for CO_2 adsorption properties, and were fully characterized to understand the deactivation mechanism over several temperature-swing (TS) adsorption-desorption cycles.

2. Experimental

2.1 Materials

For this work, CVD-grown, multi-walled carbon nanotubes (MWCNT) were purchased from ARKEMA (Graphistrength), with an average diameter of 10 - 15 nm. Graphene oxide (GO) was purchased as single layer water dispersion of 10 mg mL^{-1} (flake size 0.5 - 2.0 μm and size 0.6 - 1.2 nm) from ACS Materials. $Mg(NO_3)_2 \cdot 6H_2O$ (99%) and $Al(NO_3)_3 \cdot 9H_2O$ (98%) were purchased from Sigma-Aldrich; NaOH, H_2SO_4 (95%), HNO_3 (65%), Na_2CO_3 and K_2CO_3 were purchased from VWR international. Polycarbonate (PC) membranes were purchased from Millipore (HTTP Isopore membrane, pores diameter 0.45 μm).

2.2 Oxidation of MWCNT

In a typical oxidation procedure, 17.5 mL of concentrated H_2SO_4/HNO_3 (3:1 mixture) were added for every 500 mg of MWCNT. The mixture was stirred and refluxed for 30 min at 120 °C. After cooling, MWCNTs were vacuum-filtered over a 0.45 μm PC membrane, and base-washed with 1 L of 0.01 M NaOH. The base washing procedure assists the removal of molecular oxidation debris (also known as carboxyated carbonaceous fragments, which are thought to be related to humic or fulvic

120 acids),[46] produced during the oxidation treatment.[47, 48] In this work, only oxidized MWCNT were used,
121 and will be referred simply as to 'MWCNT'.

122 *2.3 Synthesis of Mg/Al LDH*

123 LDH platelets were synthesized by co-precipitation method; typically, aqueous solutions of
124 $Mg(NO_3)_2\ 6H_2O$ and $Al(NO_3)_3\ 9H_2O$ (0.1 and 0.05 mol respectively) were mixed and co-precipitated
125 onto a basic solution of NaOH and Na_2CO_3 (0.35 mmol and 0.09 mmol respectively). The resulting
126 white suspension was heated for 24 hours at 60 °C under vigorous stirring. The precipitate was filtered
127 using a PC membrane and washed with 1 L of water at 60 °C, in order to completely remove residual
128 sodium. The samples were then dried for 24 - 48 hours at 100 °C.

129 *2.4 Preparation of the CN supports*

130 Aqueous solutions (1 mg mL^{-1}) of GO and MWCNT were mixed at 300 rpm for 4 hours at GO/MWCNT
131 ratios of 1:0 (pure GO), 10:1, 3:1, 1:1, 1:3, 1:5 and 0:1 (pure MWCNT). The mixed solutions were then
132 filtered on PC membrane until a wet carbon paste was obtained, and used directly for LDH deposition.

133 *2.5 Deposition of LDH on CN substrates*

134 MWCNT-supported-LDH (MWCNT-LDH) and GO-supported LDH (GO-LDH) were prepared using
135 the following procedure. 100 mL of a 1 mg mL^{-1} solution of either MWCNT or GO were vacuum-
136 filtered over a 0.45 μm PC membrane until the desired low volume of carbon solution was obtained. The
137 MWCNT- (GO-) wet paste was then transferred to a 100 mL round bottom flask and 9.9 mmol of NaOH
138 and 2.5 mmol of Na_2CO_3 added. Subsequently, 1.4 mL of a salt solution of $Mg(NO_3)_2\ 6H_2O$ and
139 $Al(NO_3)_3\ 9H_2O$ (2.8 mmol and 1.4 mmol respectively) was added. The resulting black suspension was
140 aged at 60 °C for 12 hours, under vigorous stirring. The sample was filtered and dried as explained
141 above for the preparation of unsupported LDH.

142 The same procedure was applied for the preparation of hybrid GO/MWCNT-LDH materials. In order to
143 achieve a homogeneous hybridization of MWCNT and GO, the corresponding aqueous solutions were
144 mixed in the desired amounts (typically for a total volume of 200 mL) for 4 hours at room temperature.
145 The mixed solution was then filtered as described previously, and transferred to a round-bottom flask for
146 the co-precipitation of the Mg and Al salts, under basic conditions. The name of the samples includes: 1)

type of substrate (GO, MWCNT or hybrid GO/MWCNT); 2) numbers in brackets, indicating the relative proportion of GO and MWCNT; 3) subscript numbers, indicating the weight percentage (wt%) of carbon substrate (GO, MWCNT or GO+MWCNT) in the sample. For example, GO/MWCNT(1:1)$_{50}$-LDH refers to a material containing 50 wt% of a hybrid carbon substrate constituted of GO and MWCNT mixed in a ratio 1:1.

CN-LDH samples were doped with an aqueous solution of K_2CO_3 by a modified incipient wetness procedure. 1.5 mL of aqueous K_2CO_3 (0.48 M, 5% to LDH mass) were added to a fixed 100 mg of LDH and stirred for 4 hours before drying in vacuum oven at 100 °C for 24 hours.

2.6 Calcination of CN-LDH

Prior to CO_2 adsorption measurements, CN-LDH were calcined in a tubular quartz reactor (5 cm internal diameter), for 4 hours at 400 °C, under a 100 mL min^{-1} of nitrogen flow. Freshly calcined samples were submitted immediately to CO_2 adsorption measurements, or used within a day to avoid structure reconstruction driven by spontaneous adsorption of atmospheric moisture and CO_2. Further conditioning (2 h, 400 °C, 20 mL min^{-1} of nitrogen flow) occurred in the TGA before measurement.

2.7 CO_2 adsorption measurements

Multicycle CO_2 adsorption measurements were performed within a TGA (Perkin Elmer 4000) equipped with a CO_2 gas line. The sample was heated from 25 ° to 400 °C at 10 °C min^{-1} under a nitrogen flow of 60 mL min^{-1}, and held for 2 hours. Temperature was then decreased to 300 °C and the gas feed was switched to a premixed gas of 20% CO_2/N_2 and held for 1 hour. The multicycle stability of the adsorbents was assessed by performing repeated steps of CO_2 adsorption at 300 °C for 1 hour and desorption at 400 °C for 30 minutes, under nitrogen. The flow rate was kept constant at 60 mL min^{-1} throughout the experiment. Adsorption capacities were calculated from the change in mass of the adsorbents before and after the adsorption step. This response was corrected by subtracting the equivalent data from a blank empty TGA crucible, in order to take into account mass fluctuations due to change in gas density and viscosity at the feed switch and throughout the adsorption. Under the operating conditions, the fluctuation of the blank was negligible.

2.5 Measurements and characterization

Thermogravimetric analysis (TGA) was performed using a METTLER TGA/DSC1 machine (Mettler-Toledo International, Beaumont Leys Leicester, UK). Typically, 2 mg of sample were first dried at 100°C under nitrogen for 20 min and then heated from 100° to 800° at 10°C min^{-1} in 20 mL min^{-1} of air. X-ray diffraction (XRD) was carried out with a PANalytical X'Pert Pro Multi Purpose Diffractometer (Cu K_α radiation) in reflection mode, with angle (2θ) varying between 5 ° and 80 °. Transmission electron microscopy (TEM) images were obtained on a JEOL 2010, operating at 200 kV. Samples were prepared by dispersion in isopropanol (0.01 mg mL^{-1} of CN-LDH, and allowing a drop to dry onto a holey carbon copper grid (300 mesh, Agar Scientific). Scanning Electron Microscopy (SEM) images were collected using a Gemini 1525 FEGSEM, fitted with an Oxford Instruments INCA energy dispersive X-ray spectrometer (EDS). Raman spectroscopic characterisation was carried out on a Renishaw InVia Confocal Raman microscope (Renishaw plc, Wotton-under-Edge, UK). The system calibration was performed using an integrated silicon wafer prior to measurement; Raman spectra were obtained using a green laser (wavelength 532 nm, intensity 1 %, 10 seconds) in edge mode (2400 lines mm^{-1} diffraction grating); for the determination of the I_D/I_G ratio, Raman mapping was performed in StreamLine acquisition mode at *ca.* 10 μm intervals on an area of *ca.* 500 μm^2 for an acquisition of 1600 independent spectra between 1220 – 2700 cm^{-1}, using a green laser (wavelength 532 nm, 2.33 eV) 1% laser power, 10 s of exposure. The elemental composition of the adsorbents was measured by inductively coupled plasma-optical emission spectroscopy (ICP-AES) in a PerkinElmer Optima 2000 DV apparatus. The carbon component of CN-LDH samples was combusted in TGA; the metal residue was dissolved in 5 mL of *aqua regia* for 24 hours. 2 mL of the digested solution were diluted to 20 mL in deionized water, and submitted to analysis. Nitrogen adsorption and desorption isotherms were measured using a Micromeritics Tristar 3000 apparatus on 50 mg of CN-LDH samples, dried at 100°C and held overnight under N_2 prior to adsorption measurements. Specific surface areas were calculated according to the Brunauer–Emmett–Teller (BET) equation. The pore-size distribution of the samples was calculated from desorption branch using the Barrett–Joyner–Halenda (BJH) method.

3. Results and discussion

Initially, the hybrid substrates were analyzed without depositing LDH platelets; mixed substrates were prepared at different GO/MWCNT ratios of 10:1, 3:1, 1:1, 1:3, 1:5, and compared to the pure GO (1:0) and MWCNT (0:1) forms. In the XRD patterns (Fig.1a), the intensities of GO (11.3 °) and MWCNT graphitic carbon peaks (25.8 °) reflect their relative proportions in the substrates. The mean measured

thickness of the dried GO stacks was calculated from the width of the interlayer reflection using the Scherrer equation.[49] Although hybrid GO/CNT materials have been recently studied,[42, 50, 51] the degree of GO delamination, at different GO/CNT ratios, has not been reported systematically. The pure GO sample restacks on drying to an average 33 layers; however, on hybridizing with MWCNT at an optimum 1:1 ratio, the average number reduces to only 3 - 4 layers (Table 1). Hybrids with similar degree of GO layering (4 - 32 sheets) have been previously prepared by controlled LbL assembly,[51] however, the level of exfoliation reached in the present work is attributed only to the spontaneous interactions between the GO and MWCNT. This improved exfoliation, retained within the dried hybrids, is reflected in the specific surface areas calculated from N_2 adsorption-desorption measurements (Fig.1b

and Table 1). The pure MWCNT have a higher surface area than the pure GO, as they are less prone to restacking/repacking; however, their intrinsic potential surface area is lower due to the multiple shells within their structure.

Fig.1. a) XRD patterns of GO/MWCNT substrates at different compositions; b) correlation between GO exfoliation (number of layers, left axis) and specific surface area ($m^2 g^{-1}$, right axis).

Table 1

XRD calculated thickness of GO stacks, interlayer spacing and nuber of layers. Overall specific surface areas of

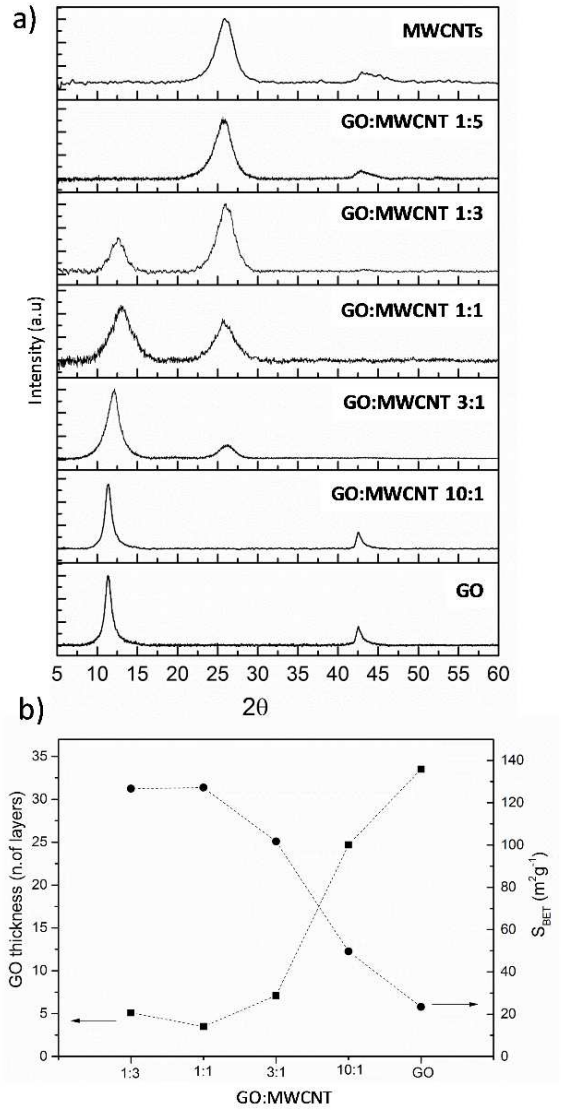

GO/MWCNT hybrid samples.

GO:MWCNT	*GO (002) (°)*	*GO stack thickness (± 0.1 nm)*	*Interlayer spacing (nm)*	*GO layers (± 0.1)*	S_{BET} *($m^2 g^{-1}$)*
MWCNT	/	/	/	/	90.34 ± 0.43
1:5	n/a	/	/	/	73.71 ± 0.19
1:3	12.67	3.6	0.70	5.1	126.63 ± 0.72
1:1	12.95	2.4	0.70	3.5	127.16 ± 0.51
3:1	12.16	4.9	0.70	7.1	101.72 ± 0.32
10:1	11.38	19.2	0.78	24.7	49.66 ± 0.19
GO	11.33	26.1	0.78	33.5	23.41 ± 0.59

The addition of a proportion of the increasingly exfoliated GO raises the average surface area, reaching a maximum for the 1:1 hybrid (127 $m^2 g^{-1}$). The synergistic improvement in surface area for mixed materials can be attributed to the MWCNT acting as spacers for the GO sheets,[39] forming a network that evenly supports the high surface area exfoliated GO layers (SEM, Fig.S1b). Similar results have been observed previously for GO/MWCNT hybrids prepared with mixing approaches,[52] although the surface areas reported are generally lower due to post-processing reduction of GO, for use in electrodes. As a control, solid GO powder was added into a MWNCT suspension to produce a phase separated network, with a distinctly different appearance (Fig.S2). TGA traces of the mixed substrates reflect the differences in their compositions (Fig.S1a); the weight loss at 200 °C of highly concentrated GO systems is associated with the removal of the surface oxides, and systematically disappears for the lower GO/MWCNT ratios.

Initially, the effects of hybridizing LDH with CN were explored using three key examples as the carbon supports: GO-, MWCNT-, and the optimal GO/MWCNT(1:1)- mixture; in each case 50 wt% LDH was combined with 50 wt% CN, to form the samples termed GO_{50}-LDH, $MWCNT_{50}$-LDH, and $GO/MWCNT(1:1)_{50}$-LDH, respectively. TGA profiles of these samples and of a reference unsupported LDH control (Fig.S3b) confirm the presence of the expected carbon and LDH components;[13] the estimated proportions (wt%, Table 2) match the nominal loadings, assuming that the combustion residues of each phase are simply additive.[13] From ICP analysis, the average Mg/Al ratio of the as-synthesized CN_{50}-LDH materials was determined as 2.1 + 0.1, which is very close to the nominal ratio of 2; the mean potassium doping was found to be 5.1 + 0.14 %, (Table 2), confirming the straightforward nature of the synthesis process. The LDH content is essentially determined by the proportion of salt precursors to nanocarbon, due to near quantitative conversion. The XRD pattern of the

unsupported LDH reference (Fig.S3a), exhibits the expected features, with narrow, symmetric and strong lines at low 2θ angles, and weaker lines at high 2θ values. The (00*l*) reflections (003), (006), (009) are easily recognized, as well as the two reflections of (110) and (113), clearly distinguished between 60 ° and 63 ° (JCPDS No. 14-191). The basal reflection (003) at 11.8 ° falls approximately at the same 2θ angle as the GO layer spacing (11.4 °), although the GO peak is weak and tends to diminish further after hydrothermal treatment (LDH synthesis conditions),[15] due to elimination of the oxidative debris. The graphitic carbon (002) at 26.3 ° is isolated from the other peaks. For CN_{50}-LDH, the (003) peak broadens compared to the unsupported sample (Table 2). This effect can be attributed to a reduced crystallite size in the stacking direction (*c*-direction) from 22 nm for pure LDH to 5.7 - 15 nm for CN_{50}-LDH, due to CN modifying the nucleation/growth conditions.[13, 15]

Table 2

Summary table of samples composition, morphologic characteristics and CO_2 adsorption properties.

[a] LDH platelet thickness calculated from the (003) peak by Scherrer equation. [b] gas adsorption capacity relative to the 1st adsorption cycle.

Sample	C wt% (nom)	C wt% (actual)	Mg/Al (mol/mol)	K (wt%)	LDH platelet thickness[a] (nm)	S_{BET} ($m^2\ g^{-1}$)	V_{pores} ($cm^3\ g^{-1}$)	CO_2 adsorbed (mol kg^{-1}LDH)	Rel capacity[b] 20th cycle (%)
LDH	0	0	2.2	5.1	22.8	49.31 ± 0.63	0.32	0.18 ± 0.02	50
$MWCNT_{50}$-LDH	50	48	2.1	4.9	15	77.69 ± 1.98	0.31	0.24 ± 0.03	77
GO_{50}-LDH	50	46	2.2	5.3	5.7	84.89 ± 0.17	0.27	0.27 ± 0.02	65
$GO/MWCNT(1:1)_{50}$ -LDH	50	46	1.9	5.1	13.7	103.51±0.36	0.41	0.49 ± 0.01	96

A change in crystallinity may also contribute to the peak width, although LDH crystallinity is usually dictated by temperature, ageing time, pH and mixing rate,[53, 54] factors that were kept consistent between batches. Peak broadening is much more noticeable for the GO_{50}-LDH sample than for $MWCNT_{50}$-LDH (LDH platelet thickness of 5.7 nm and 15 nm, respectively); the two dimensional GO sheets should be more compatible with the LDH platelets than the MWCNT.[15] The LDH platelet thickness of the GO/$MWCNT_{50}$-LDH hybrid (13.7 nm) is intermediate between GO- and MWCNT-LDH. No crystalline signal for the potassium carbonate promoter was detected, consistent with the low loading introduced

(5%) and a homogenous distribution. In principle TEM can help to confirm platelet thickness, but is difficult to apply, with statistical significance to LDH supported on convoluted GO; qualitatively, however, TEM (Fig.S4) indicates a similar LDH platelet thickness as the XRD results. SEM and TEM images confirm an intimate association between LDH particles and the carbon substrates, with LDH aggregates covering the surface of the GO (Fig.2a,d), MWCNT (Fig.2b,e) and the hybrid (Fig.2c,f). Importantly, the GO/MWCNT$_{50}$-LDH hybrid manifests enhanced specific surface area compared to both GO$_{50}$-LDH and MWCNT$_{50}$-LDH (Table 2), continuing the trend identified above for the supports in the absence of LDH (Fig.1). Previous work suggests that the 2D geometry of GO sheets may offer a more compatible nucleation surface for the LDH platelets,[13] however, there is no evidence of selective growth in the GO/MWCNT-LDH material. The similar concentration of oxygen functionalities (1 - 2 mmol g^{-1})

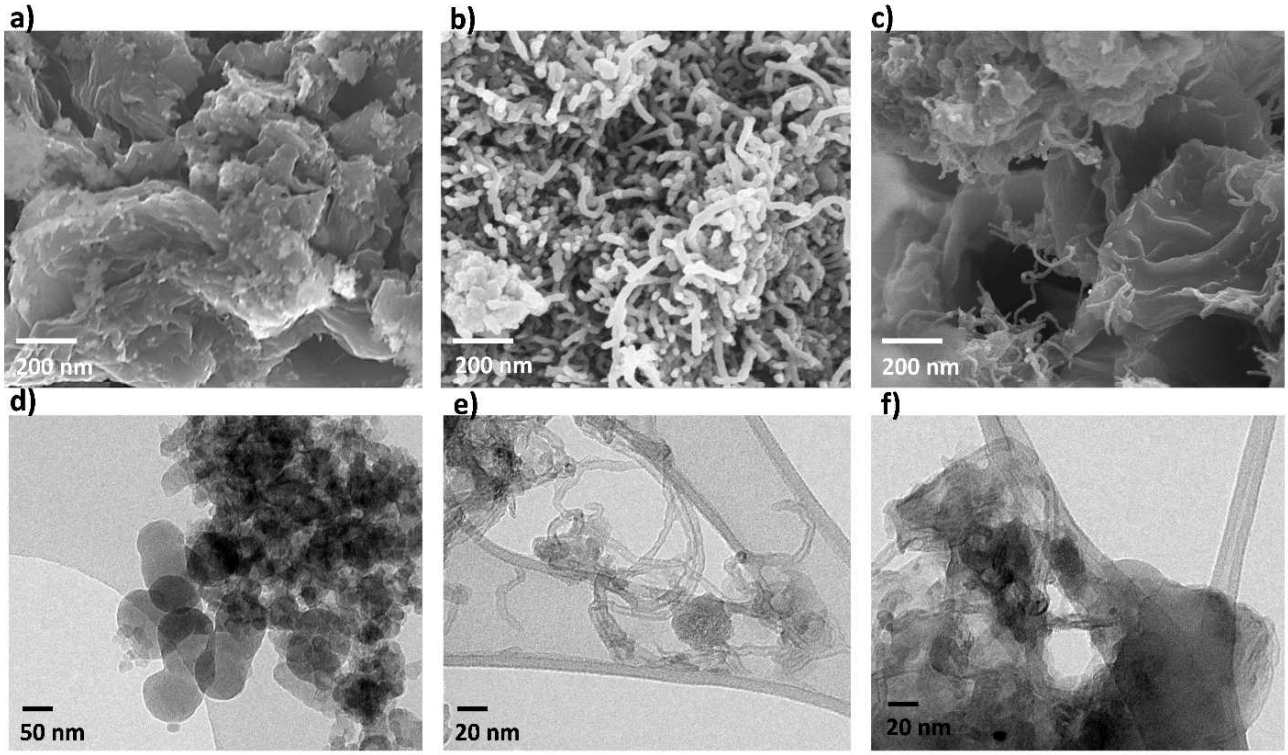

for both GO and MWCNT,[15, 47] may dominate the nucleation process.

Fig.2. SEM and TEM images of a,d) GO$_{50}$-LDH; b,e) MWNT$_{50}$-LDH; c,f) GO/MWCNT(1:1)$_{50}$-LDH samples.

The properties of the CN$_{50}$-LDH materials as CO_2 adsorbents were assessed over 20 cycles of gas adsorption-desorption. All the samples manifested fast intrinsic CO_2 adsorption kinetics (Fig.3a), achieving more than 80% of their equilibrium capacity within 30 minutes. Critically, the

GO/MWCNT$_{50}$-LDH hybrid exhibited the highest gas adsorption capacity (0.49 mol CO_2 kg^{-1}LDH), more than twice the value of unsupported LDH (0.18 mol CO_2 kg^{-1}LDH), and significantly higher than LDH supported on GO and MWCNT independently (0.27 and 0.24 mol CO_2 kg^{-1}LDH, respectively). The first-contact adsorption capacity of the GO$_{50}$-LDH sample is higher than the MWCNT$_{50}$-LDH one, in accordance with previous results.[15] Under these operating conditions, the GO/MWCNT substrate alone has a negligible CO_2 adsorption (0.02 mol CO_2 kg^{-1} carbon) compared to the LDH component (Fig.3a). Previous studies have also shown very low capacity on either raw or acid treated nanocarbons, and have ruled out any contribution potentially arising from residual catalyst particles.[55]

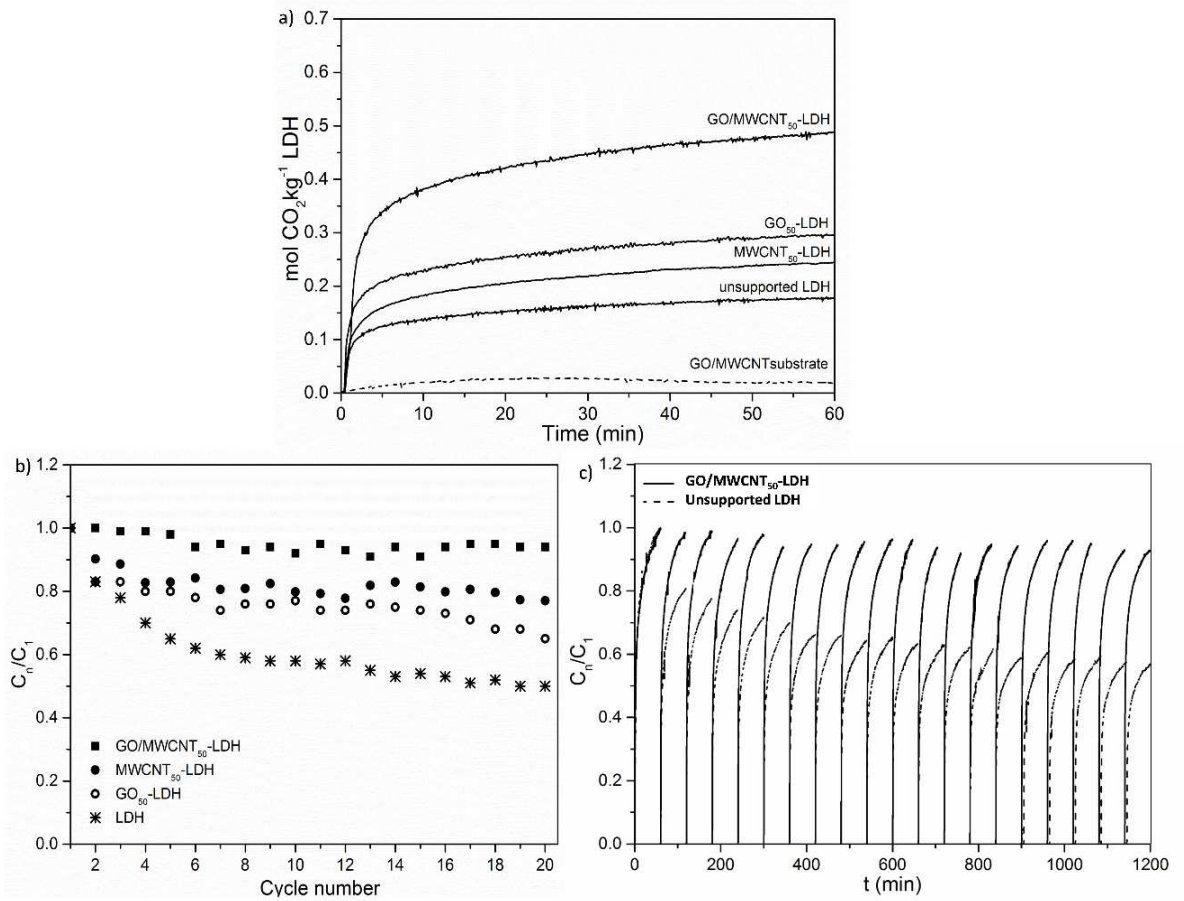

Fig.3. a) First-cycle CO_2 adsorption profiles of unsupported/supported LDH and GO/MWCNT (1:1) substrate, at 300 °C and P_{CO2}= 0.2 bar, after blank subtraction (pan+substrate). Substrate curve refers to mol CO_2 kg^{-1} of carbon; b) normalized CO_2 adsorption capacity over 20 adsorption-desorption cycles; c) multicycle profiles of activated GO/MWCNT(1:1)$_{50}$-LDH and unsupported-LDH samples. Values are listed in Table 2

The adsorption capacity of all the samples showed good reproducibility among three repeated measurements for each sample (standard deviation of 0.01 - 0.03 mol CO_2 kg^{-1}LDH). The improved gas adsorption capacity manifested by GO/$MWCNT_{50}$-LDH can be attributed to the presence of the high surface area hybrid support and the enhanced effective LDH surface area, due to changes in crystal size and quality (Table 2). Smaller supported-LDH platelets are thought to have a higher concentration of active edge sites, which were previously shown to provide the binding sites for CO_2 adsorption.[9] There is a synergy between the MWCNT, which provide a robust open network, and the GO, which is geometrically compatible with LDH.

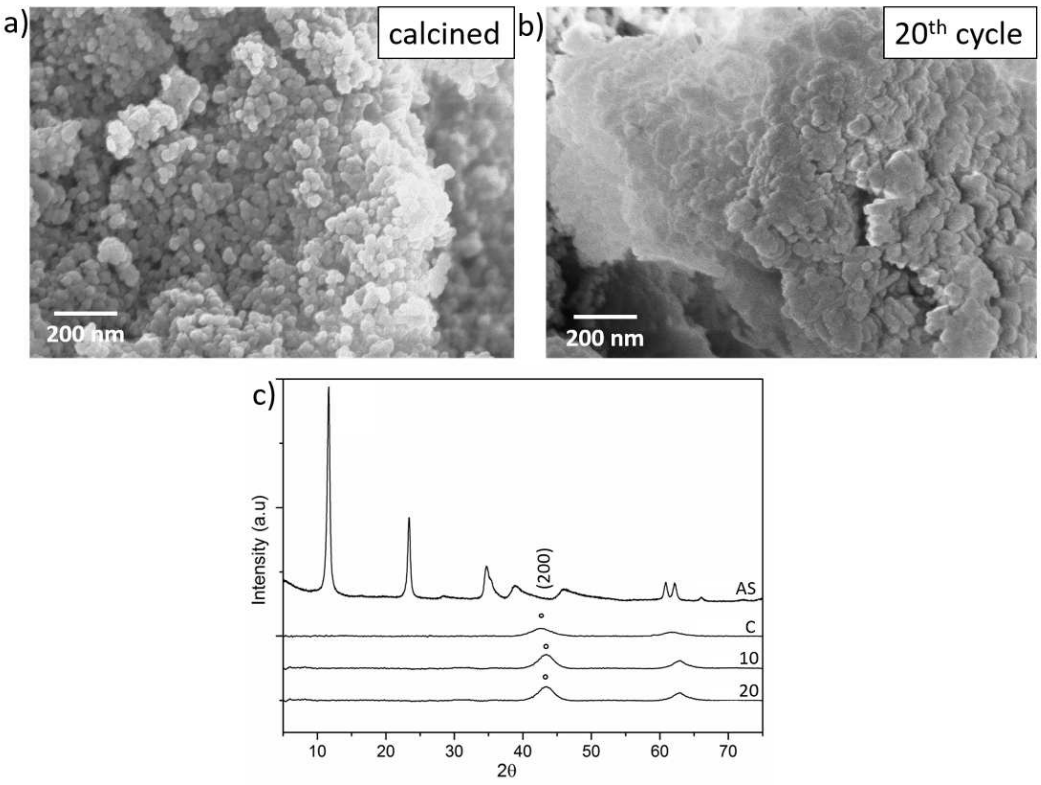

Fig.4. SEM images of unsupported LDH materials: a) calcined, b) at the 20th cycle of gas adsorption-desorption; c) XRD evolution of unsupported LDH at different stages of the adsorption-desorption test: as-synthesised (AS), calcined (C) materials, after 10, and after 20 cycles.

The regeneration and stability of the adsorbents were also assessed by carrying out continuous adsorption-desorption cycles under dry conditions (Fig.3b-c). Unsupported LDH materials are known to suffer from irreversible declines in the adsorption capacity over cycling,[16] due to chemisorption phenomena and particle sintering.[56] The present, unsupported LDH sample follows a similar decreasing

trend to previous reports (Fig.3b,c), exhibiting a loss of *ca.* 50 % of adsorption capacity at the 20th cycle. This trend is associated with a progressive sintering of the LDH platelets (SEM images, Fig.4), which likely contributes to the loss of surface area and basic site availability. However, this poor multicycle stability is mitigated by supporting LDH on either GO or MWCNT, but only partially. In contrast, the GO/MWCNT(1:1)$_{50}$-LDH hybrid retains up to 96% of its initial CO_2 adsorption capacity throughout all the 20 cycles of testing. This exceptionally stable behavior has not been observed before for adsorptions under dry conditions, and suggests the presence of a synergistic effect of the MWCNT and GO. The presence of modest levels of dopants were previously shown not to affect the multicycle stability of the materials, but only the absolute capacity.[16]

To provide an explanation for this retained stability, the morphological evolution of LDH and CN$_{50}$-LDH samples was studied, *via* XRD, SEM and Raman spectroscopy (Fig.5,6,7), at different stages of the multicycle adsorption tests, specifically as-synthesized (AS), calcined (C), after 10 cycles and after 20 sorption cycles. Cycling adsorption-desorption tests on unsupported LDH caused the structure to progressively lose surface area, likely due to continuous decarbonation, irreversible chemisorption effects, sintering or carbon deposition.[56] The calcined particles were found to sinter into larger structures, as calculated from the width of the (200) peak of periclase in XRD (Fig.5, and Table in Fig.S4), eventually halving the initial adsorption capacity.

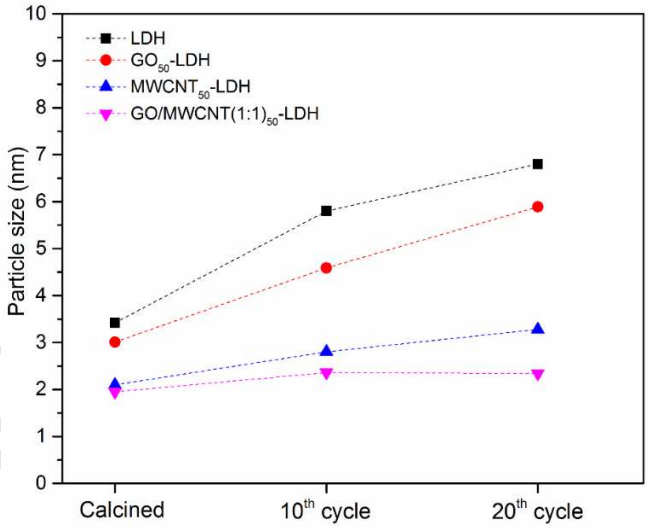

Fig.5. Graph of MMO particle size for calcined unsupported LDH and CN$_{50}$-LDH at different stages of the multicycle adsorption process. The reduced slope of the curve evidences reduced sintering effects.

The GO_{50}-LDH material exhibits significant structural changes following the thermal cycling (Fig.6a). On calcination, GO is thermally 'reduced' leading to restacking and the appearance of the (002) graphitic peak at ~26.4 °; at the same time, peaks associated with free K_2CO_3 appear, indicating that some of the impregnated salt was associated with the lost GO oxygen moieties, as expected due to acid-base interactions. By the 10th cycle, the intensity of the graphitic (002) peak is significantly decreased and eventually lost by the 20th cycle, consistent with the disappearance of the characteristic G and D bands from the Raman spectra, which are normally associated with graphitic structures (Fig.7a). Previous work reported that heat treatments of Ni/Mn LDH/GO hybrids at high temperatures (450 - 800 °C) in inert atmosphere caused gasification and removal of the graphitic material.[57] Here, the temperature is modest, but apparently sufficient to cause a similar loss of the graphitic component. The loss of carbon is supported by TGA (Fig.S5), showing that the carbon content in the GO-LDH material drops from 46 wt% before cycling (Table 2) to *ca* 6 wt% afterwards. Towards the end of the cycling experiment, the potassium redistributes into the periclase phase,[58] indicated by the disappearance of the initial K_2CO_3 peaks in XRD pattern (Fig.6a). The degradation of the GO substrate and associated loss of support, allows the MMO particles to sinter, increasing their size as estimated from peak width (Fig.5 and S4), though at a slower rate than the pure LDH. These observations account for the 30% capacity loss measured for GO_{50}-LDH after 20 cycles. Although GO appears not to be an ideal substrate for LDH, it slows the deactivation of the adsorbent due to sintering, both in rate and in extent.

For $MWCNT_{50}$-LDH (Fig.6b), the initial calcined structure is better retained over cycling compared to GO_{50}-LDH, as the carbon (002) and periclase (200) reflections are present in all the XRDs. Though reduced in intensity, the XRD carbon peak and the typical Raman features of MWCNT are still detected at the final adsorption cycle (Fig.7b). However, a more defective structure is confirmed by the increased I_D/I_G ratio of the cycled sample (Table Fig.7d), and the partial loss of G band splitting. There appears to be insufficient K_2CO_3, associated with the much smaller oxidized MWCNT surface, to nucleate separate salt crystals. Overall, the MWCNT network is more robust than GO, unsurprisingly as only the surface is initially oxidised, leaving a lower surface area and more perfect graphitic core that appears not to gasify as readily as the GO. Thus, the sintering of the sorbent particles is reduced compared to unsupported LDH and GO_{50}-LDH (Fig.4 and 5). These observations are in turn reflected by the greater retained adsorption capacity (75%) manifested by the $MWCNT_{50}$-LDH sample in the last cycle.

The GO/MWCNT(1:1)$_{50}$-LDH hybrid benefits from the presence of both types of CN. Whilst the GO is reduced (no layer peak at 11.4°), the XRD pattern of the calcined hybrid is relatively little altered during

subsequent cycling (Fig.6c), and the graphitic Raman band is better retained compared to either pure case (Fig.7c). In the GO/MWCNT(1:1)$_{50}$-LDH hybrid, the MWCNT and the GO appear to act synergistically. One possible explanation is that the large flat GO flakes, coated in LDH, provide a barrier offering a degree of protection to the MWCNT, whilst the MWCNT maintain a network scaffolding that limits sintering of the LDH/periclase that otherwise leads to exposure of the (reduced) GO framework. The microstructure of the hybrid, shown in the SEM images (Fig.6c), indeed exhibits much coarser plate-like features than the MWCNT$_{50}$-LDH, but more separated into discrete particles than the GO$_{50}$-LDH. This stable, hybrid support shows very little sintering of the periclase particles (Fig.5 and S4), consistent with the excellent retention of the capacity (96%) across the 20 cycles.

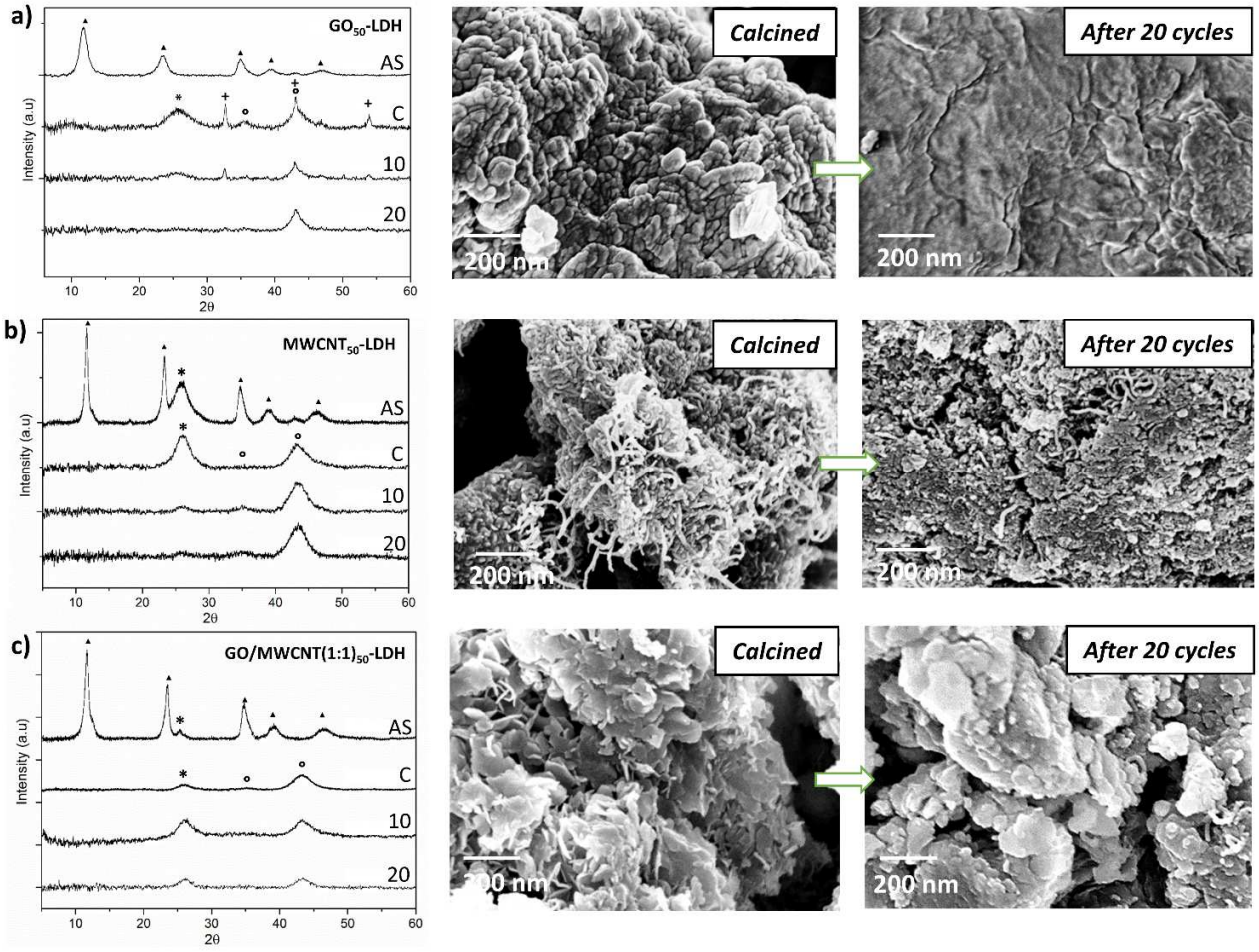

Fig.6. XRD patterns of a) GO$_{50}$-LDH, b) MWCNT$_{50}$-LDH, c) GO/MWCNT(1:1)$_{50}$-LDH at different stages: as-synthesized (AS) and calcined (C) materials, after 10, and after 20 cycles of gas adsorption-desorption. (▲) LDH reflections, (*) graphitic carbon, (°) periclase, (+) potassium carbonate. SEM images of calcined samples and after cycling 20 times.

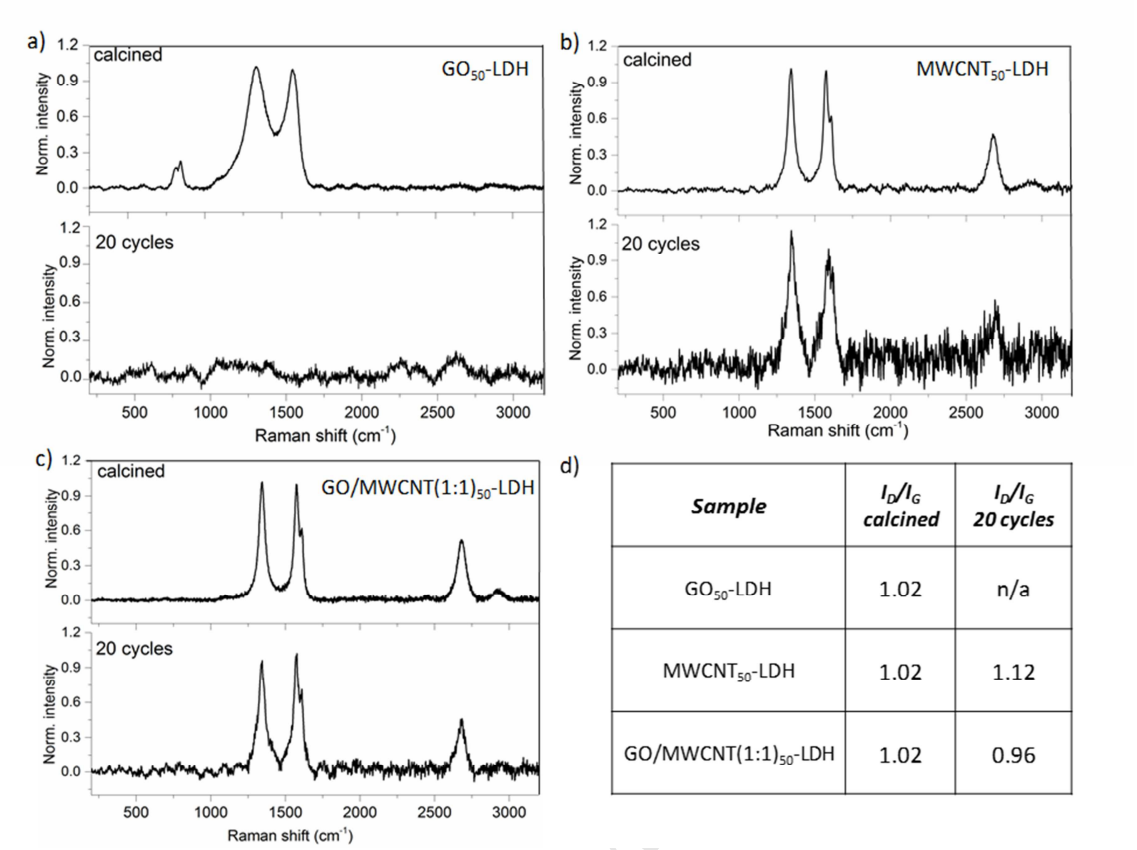

d)

Sample	I_D/I_G *calcined*	I_D/I_G *20 cycles*
GO_{50}-LDH	1.02	n/a
$MWCNT_{50}$-LDH	1.02	1.12
GO/$MWCNT(1:1)_{50}$-LDH	1.02	0.96

Fig.7. Raman spectra at λ_{laser} of 532 nm of activated (calcined) materials and after 20 cycles of gas adsorption/desorption for a) GO_{50}-LDH, b) $MWCNT_{50}$-LDH and c) GO/$MWCNT(1:1)_{50}$-LDH materials. Spectra are normalized to the G mode at *ca.* 1575 nm. d) Table with calculated I_D/I_G ratios.

Having established a synergistic response, the influence of different ratios of GO and MWCNT on the final CO_2 adsorption properties were explored at a range of GO/MWCNT compositions (1:5, 1:3, 1:1, 3:1). The GO/MWCNT substrate of composition 10:1 resulted in poor hybridization and low surface area (see Fig.1), and was not investigated further. The other hybrid substrates were added to LDH at various fractions (50, 30, 20 carbon wt%), producing supported hybrids denoted as GO/$MWCNT_{50}$-LDH, GO/$MWCNT_{30}$-LDH and GO/$MWCNT_{20}$-LDH, respectively. Lower loadings of the inert supports are more appealing industrially speaking, since they reduce the size of the adsorption units and limit the overall costs; in addition, the previous optimums for the pure GO and pure MWCNT supports were at 50 wt% carbon, or less. Generally, these three phase hybrids were formed successfully (XRD, Fig.S6). LDH grown on low GO/MWCNT ratio supports display broader XRD (003) peaks, and

thus smaller platelet thickness in the *c*-direction (Fig.8a and S6), which is consistent with the formation of a well hybridised material and the initial trends discussed above.

First contact CO_2 adsorption capacity and multicycle stability were assessed as previously, and compared to BET surface area data (Fig.S7). The results can be summarized as follows: 1) the adsorption kinetics for all the adsorbents is very fast, with 80% of the equilibrium capacity reached again in the first 10 minutes of gas exposure (Fig.S8a,c,e); 2) regardless of the proportion of the support added to the LDH phase, the highest intrinsic CO_2 adsorption capacity is always exhibited by LDH supported on a GO/MWCNT substrate of composition 1:1 (Fig.8b-d); 3) LDH deposited on the GO/MWCNT (1:1) substrate also manifest the highest surface areas within each set of carbon loadings; 4) for each set of samples, the CO_2 uptake trend is consistent with the BET surface area of the adsorbents (Fig.8b-d).

Fig.8. a) Crystallite size of the adsorbents per support type. Specific surface area ($m^2 g^{-1}$) and CO_2 uptake (mol CO_2 per mass of LDH) *vs* support type for b) GO/$MWCNT_{50}$-LDH, c) GO/$MWCNT_{30}$-LDH, d) GO/$MWCNT_{20}$-LDH (values in Table S2). The error bars for the BET are very small (as indicated in the tabulated data, Table S1), and mostly negligible on the scale of the plots.

411

412 The specific surface area of the hybrids is related to the level of GO exfoliation/MWCNT intercalation
413 achieved, and reflects the results for the pure nanocarbon blends. The enhancement in the intrinsic
414 adsorption capacity (*i.e.* per mass of LDH) is important from a fundamental perspective; however, in
415 practical terms, it is also important to consider the adsorption capacity per mass of total adsorbent (*i.e.*
416 LDH+GO+MWCNT). The 3d plots of all the sorption data (Fig.9) confirm the optimum substrate
417 composition GO/MWCNT 1:1 (blue bars), and highlights that, across all the GO/MWCNT ratios, the
418 optimum carbon loading is between 10 - 20 wt% (0.46 mol CO_2 kg^{-1} ads for the
419 GO/MWCNT(1:1)$_{20}$-LDH hybrid), lower than previously used support fractions.[12, 13] This range takes
420 advantage of improved dispersion and gas accessibility without increasing significantly the total mass of

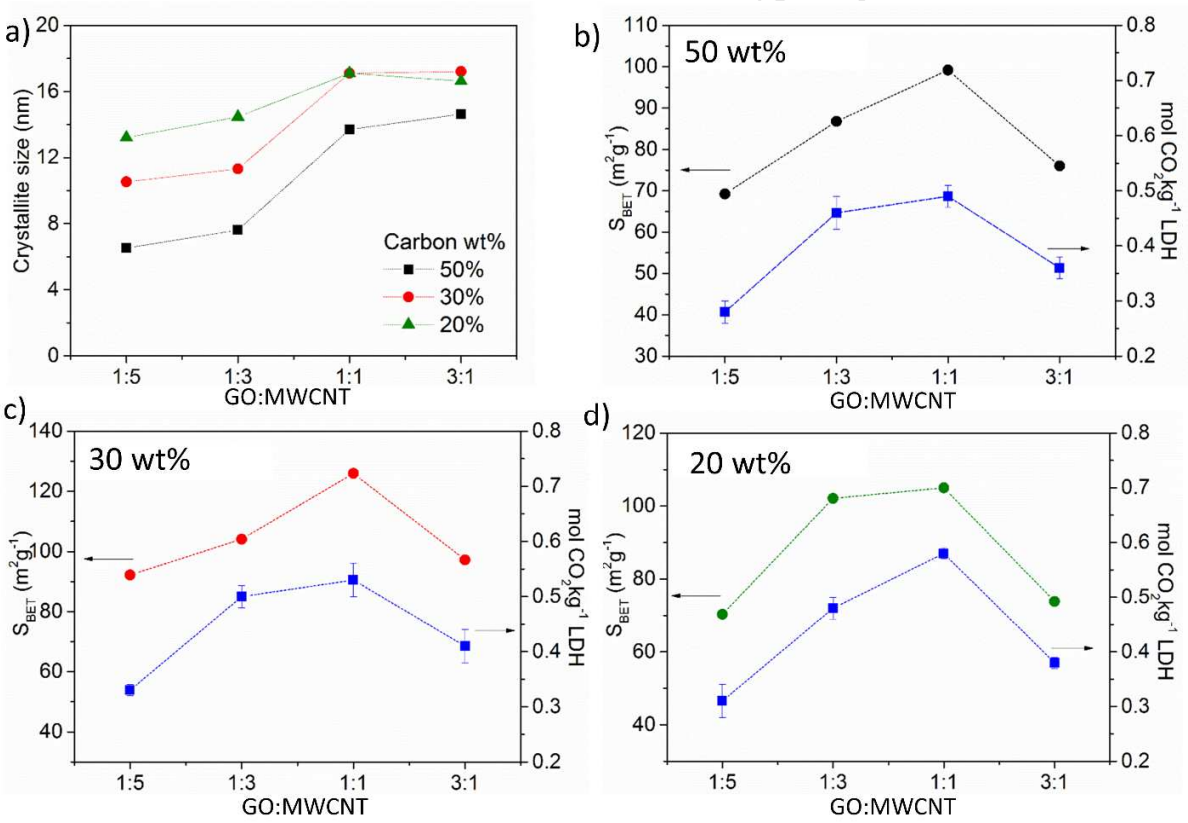

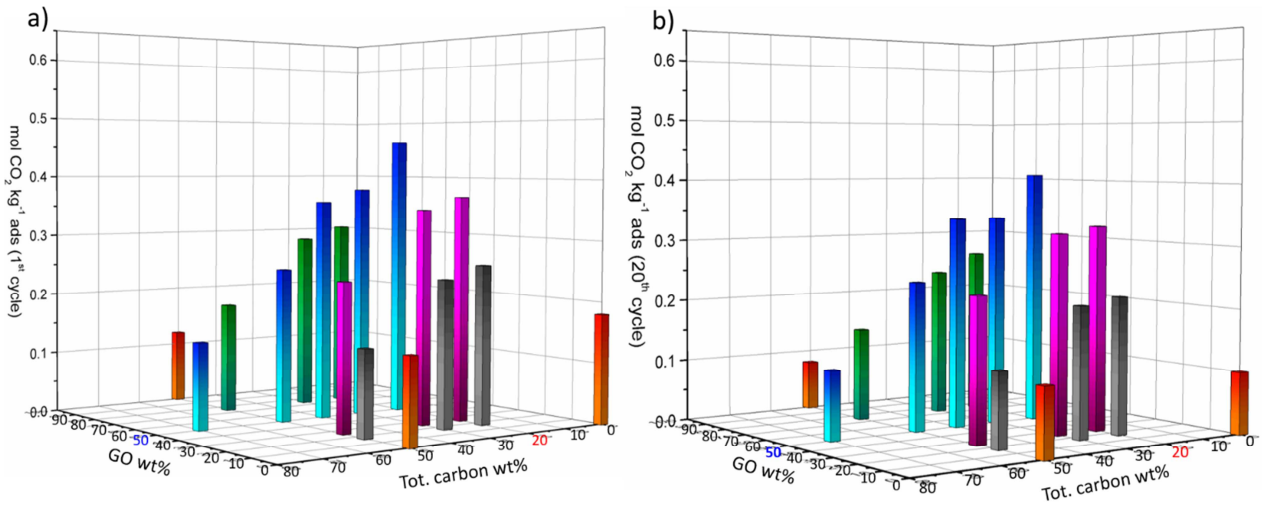

adsorbent. The existence of an optimum carbon loading, when normalising to the total mass of sorbent, was reported previously both for the pure MWCNT-LDH (optimum at 35 – 50 wt% MWCNT)[13] and pure GO-LDH (optimum at 5 - 10 wt% GO)[15] systems. As expected, the optimum loading for the hybrid GO/MWCNT-LDH falls between the two previous values, although much closer to the GO-LDH, due to the greater specific surface area of GO once restacking is prevented. Once isolated, a relatively small fraction of GO is sufficient to support all the LDH platelets. After 20 cycles (Fig.9b and S8), the adsorption capacity per mass of adsorbent continues to exhibit a marked improvement for all GO/MWCNT supported LDH samples compared to both pure LDH and LDH supported on only GO or MWCNT (red bars). The optimum performance is still observed for equal proportions of GO and MWCNT, for all contents of LDH. The capacity loss in the best cases, was only between 4% and 9%, much lower than previous reports for other supported HTs, under dry conditions.

Fig.9. CO_2 adsorption capacity per total mass of *adsorbent* at a) 1st cycle and b) 20th cycle, for all the samples. The data show consistent trends across a large number of samples, confirming the hybrid effect.

The absolute CO_2 adsorption capacity of the CN-LDH hybrids, though greatly improved compared to unsupported LDH, remains on an average 0.4 - 0.5 mol CO_2 kg^{-1} adsorbent. This range is lower than other types of commercially-available solid adsorbents, for example 0.1 - 5 mol CO_2 kg^{-1} zeolite and 0.1 - 3.5 mol CO_2 kg^{-1} activated carbons, tested at their active temperature of 5 – 100 °C.[10] However, as

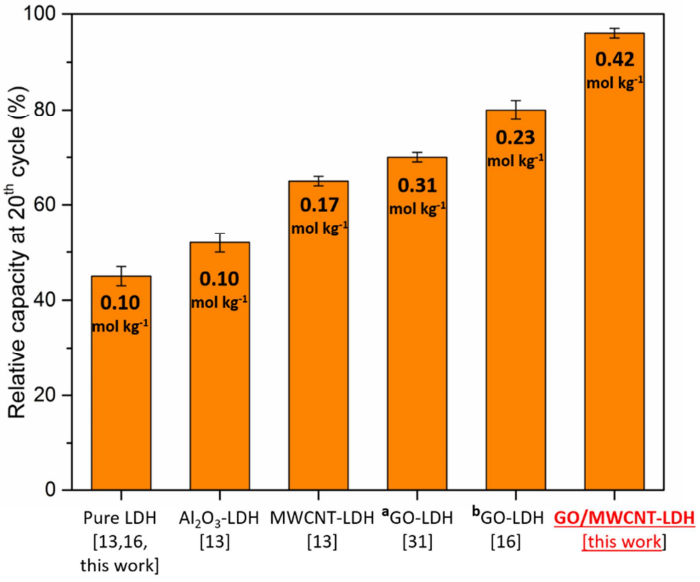

noted in the introduction, CN-LDH materials can successfully operate at much higher temperatures (200 – 400 °C), with good kinetics and potentially over long cycle lives. Moreover, they require low

energy in regeneration (300 - 400 °C), as opposed to other high temperature solid adsorbents ($LiZrO_3$ and CaO systems) which, although possessing higher adsorption capacities, can be regenerate only above 600 – 800 °C, and manifest slower adsorption kinetics. The 20 cycles tested in this study were selected to allow practical evaluation of a large number of hybrids, using a common range in the scientific literature; clearly industrial evaluation would require extensive studies across a range of more realistic conditions. Nevertheless, the 96 % retention of sorption capacity is a striking improvement over previous studies (Fig.10), and the absolute amount gas sorption in the last cycle is also significantly higher (0.42 mol CO_2 kg^{-1} ads) than recent reports. It is worth noting that Meis *et al.* reported a stable cycling behaviour of their CNF-supported LDH,[12] but under wet conditions (wet CO_2 gas feed (83% N_2/12 % H_2O/5 % CO_2), which are known to obscure any specific stabilising effect of the support.[48] In the present case, the increased stability in dry-feed conditions can be directly attributed to the presence of the carefully designed high surface area and robust substrates.

Fig.10. Summary of comparable data for recently reported Mg/Al CO_3 LDH materials: CO_2 adsorption capacity retention (per mass of total adsorbent and relative to the 1st contact adsorption) at the 20th adsorption cycle. Examples considered include only materials tested under similar operative conditions (dry gas feed, 1 atm, medium temperatures of 200-400 °C). [a] Mg/Al NO_3 LDH type, [b] Mg/Al CO_3 LDH type.

4. Conclusions

The use of a hybrid GO/MWCNT support for Layered Double Hydroxides offers a clear synergistic benefit in CO_2 adsorption applications. This synergy can be considered as a true "hybrid effect", highlighting the benefit of combining phases such that the mixed phase performs better than either pure phase or a simple rule of mixtures. Compared to substrates consisting of a single nanocarbon species, the mixed GO/MWCNT systems are more effective, more stable, and offer a higher specific surface area for the active LDH material. Systematic investigation consistently identified equal proportions of GO and MWCNT (ratio 1:1) as the optimum composition to maximize both accessible surface area and sorption performance. Indeed, the surface area was found to correlate directly with the CO_2 uptake. Both MWCNT and GO contribute to the surface area and can support the LDH platelets; however, the primary role of the MWCNT is to form a compatible, robust network, preventing restacking of the GO; a high degree of exfoliation is therefore retained in the GO phase, providing a large surface anionic area with a 2d geometry, particularly suited to the nucleation and growth of smaller cationic LDH platelets.

When exfoliated, GO sheets are a more efficient support than MWCNT. The presence of an open, accessible, high surface area network stabilizes the final adsorbent, minimizing the deactivation and sintering effects normally observed for unsupported LDH. Careful processing was required to generate the intimate, uniform, three phase mixture that ensures an effective hybrid response. The best hybrid identified (GO/MWCNT$(1:1)_{20}$-LDH) had an intrinsic adsorption capacity of 0.58 mol CO_2 kg^{-1} LDH, corresponding to 0.46 mol CO_2 kg^{-1} of total adsorbent. The good performance per overall weight of sorbent is particularly noteworthy, since many previous studies used much higher dilutions of LDH on the support, increasing the weight significantly. Most strikingly, the intrinsic CO_2 adsorption capacity of the hybrids was exceptionally consistent over repeated cycles of gas adsorption-desorption, even under dry conditions, retaining up to 96% of the initial sorption capacity after twenty cycles, significantly more than both unsupported LDH (50% retained) and previous reports for supported LDH (60 - 85%). This type of hybrid sorbent may be considered, in the long term, for targeted pre-combustion carbon capture applications, for instance in sorption enhanced water gas shift reactions and sorption enhanced methane reforming, but may also be applied to smaller scale sorption problems. The improved performance of the supported LDH is likely to be relevant to other known LDH applications, including as heterogeneous bases for catalysis, as sorbents for the desulphurization of fuel,[59] and in pseudocapacitors.[29] In addition, the concept of a GO/MWCNT hybrid network as substrate can be readily extended to other adsorbent materials, particularly where problems of sorbent degradation over use are still present.[60] Other forms of 1d/2d hybrid materials can also be considered, drawing on the growing body of nanomaterial feedstocks considered to be analogous to graphene/nanotubes.[61-63]

Acknowledgements

The authors would like to thank prof. David Chadwick for help and discussion and Dr Hannah Leese for TEM images acquisition. Financial support for this project was provided by the Deanship of Scientific Research at King Abdulaziz University (Grant D-1- 434), and EPSRC grant EP/L001896/1.

References

1. Duan, X., Evans, David G., *Layered Double Hydroxides,*. Springer-Verlag Berlin: Berlin, **2006**, 193–223.
2. Centi, G.; Perathoner, S., Catalysis by layered materials: A review. *Microporous and Mesoporous Materials* **2008,** 107, (1–2), 3-15.
3. Nakayama, H.; Wada, N.; Tsuhako, M., Intercalation of amino acids and peptides into Mg–Al layered double hydroxide by reconstruction method. *International Journal of Pharmaceutics* **2004,** 269, (2), 469-478.

4. Tronto, J.; Reis, M. J. d.; Silvério, F.; Balbo, V. R.; Marchetti, J. M.; Valim, J. B., In vitro release of citrate anions intercalated in magnesium aluminium layered double hydroxides. *Journal of Physics and Chemistry of Solids* **2004,** 65, (2–3), 475-480.

5. Becker, C. M.; Dick, T. A.; Wypych, F.; Schrekker, H. S.; Amico, S. C., Synergetic effect of LDH and glass fiber on the properties of two- and three-component epoxy composites. *Polymer Testing* **2012,** 31, (6), 741-747.

6. Yong, Z.; Rodrigues, A. r. E., Hydrotalcite-like compounds as adsorbents for carbon dioxide. *Energy Conversion and Management* **2002,** 43, (14), 1865-1876.

7. De Luca, F.; Menzel, R.; Blaker, J. J.; Birkbeck, J.; Bismarck, A.; Shaffer, M. S. P., Nacre-nanomimetics: Strong, Stiff, and Plastic. *ACS Applied Materials & Interfaces* **2015,** 7, (48), 26783-26791.

8. Yong, Z.; Mata; Rodrigues, A. E., Adsorption of Carbon Dioxide onto Hydrotalcite-like Compounds (HTlcs) at High Temperatures. *Industrial & Engineering Chemistry Research* **2001,** 40, (1), 204-209.

9. Ram Reddy, M. K.; Xu, Z. P.; Lu, G. Q.; Diniz da Costa, J. C., Layered Double Hydroxides for CO_2 Capture: Structure Evolution and Regeneration. *Industrial & Engineering Chemistry Research* **2006,** 45, (22), 7504-7509.

10. Choi, S.; Drese, J. H.; Jones, C. W., Adsorbent Materials for Carbon Dioxide Capture from Large Anthropogenic Point Sources. *ChemSusChem* **2009,** 2, (9), 796-854.

11. Wang, Q.; Luo, J.; Zhong, Z.; Borgna, A., CO_2 capture by solid adsorbents and their applications: current status and new trends. *Energy & Environmental Science* **2011,** 4, (1), 42-55.

12. Meis, N. N. A. H.; Bitter, J. H.; de Jong, K. P., Support and Size Effects of Activated Hydrotalcites for Precombustion CO_2 Capture. *Industrial & Engineering Chemistry Research* **2010,** 49, (3), 1229-1235.

13. Garcia-Gallastegui, A.; Iruretagoyena, D.; Mokhtar, M.; Asiri, A. M.; Basahel, S. N.; Al-Thabaiti, S. A.; Alyoubi, A. O.; Chadwick, D.; Shaffer, M. S. P., Layered double hydroxides supported on multi-walled carbon nanotubes: preparation and CO_2 adsorption characteristics. *Journal of Materials Chemistry* **2012,** 22, (28), 13932-13940.

14. Abolghasemi, M. M.; Yousefi, V.; Piryaei, M., Synthesis of carbon nanotube/layered double hydroxide nanocomposite as a novel fiber coating for the headspace solid-phase microextraction of phenols from water samples. *Journal of Separation Science* **2015,** 38, (8), 1344-1350.

15. Garcia Gallastegui, A.; Iruretagoyena, D.; Gouvea, V.; Mokhtar, M.; Asiri, A. M.; Basahel, S. N.; Al-Thabaiti, S. A.; Alyoubi, A. O.; Chadwick, D.; Shaffer, M. S. P., Graphene Oxide as support for Layered Double Hydroxides: enhancing the CO_2 sorption capacity. *Chemistry of Materials* **2012,** 24 (23), 4531–4539.

16. Iruretagoyena, D.; Shaffer, M. S. P.; Chadwick, D., Layered Double Oxides Supported on Graphene Oxide for CO_2 Adsorption: Effect of Support and Residual Sodium. *Industrial & Engineering Chemistry Research* **2015,** 54 (26), 6781–6792.

17. Aschenbrenner, O.; McGuire, P.; Alsamaq, S.; Wang, J.; Supasitmongkol, S.; Al-Duri, B.; Styring, P.; Wood, J., Adsorption of carbon dioxide on hydrotalcite-like compounds of different compositions. *Chemical Engineering Research and Design* **2011,** 89, (9), 1711-1721.

18. Othman, M. R.; Rasid, N. M.; Fernando, W. J. N., Mg–Al hydrotalcite coating on zeolites for improved carbon dioxide adsorption. *Chemical Engineering Science* **2006,** 61, (5), 1555-1560.

19. Salvetat, J.-P.; Briggs, G. A. D.; Bonard, J.-M.; Bacsa, R. R.; Kulik, A. J.; Stöckli, T.; Burnham, N. A.; Forró, L., Elastic and Shear Moduli of Single-Walled Carbon Nanotube Ropes. *Physical Review Letters* **1999,** 82, (5), 944-947.

20. Salvetat, J. P.; Bonard, J. M.; Thomson, N. H.; Kulik, A. J.; Forró, L.; Benoit, W.; Zuppiroli, L., Mechanical properties of carbon nanotubes. *Applied Physics A* **1999,** 69, (3), 255-260.

21. Hone, J.; Whitney, M.; Piskoti, C.; Zettl, A., Thermal conductivity of single-walled carbon nanotubes. *Physical Review B* **1999,** 59, (4), R2514-R2516.

22. Javey, A.; Guo, J.; Wang, Q.; Lundstrom, M.; Dai, H., Ballistic carbon nanotube field-effect transistors. *Nature* **2003,** 424, (6949), 654-657.

23. Peigney, A.; Laurent, C.; Flahaut, E.; Bacsa, R. R.; Rousset, A., Specific surface area of carbon nanotubes and bundles of carbon nanotubes. *Carbon* **2001,** 39, (4), 507-514.

24. Nardecchia, S.; Carriazo, D.; Ferrer, M. L.; Gutierrez, M. C.; del Monte, F., Three dimensional macroporous architectures and aerogels built of carbon nanotubes and/or graphene: synthesis and applications. *Chemical Society Reviews* **2013,** 42, (2), 794-830.
25. Khan, S. A.; Khan, S. B.; Asiri, A. M., Toward the design of Zn-Al and Zn-Cr LDH wrapped in activated carbon for the solar assisted de-coloration of organic dyes. *RSC Advances* **2016,** 6, (86), 83196-83208.
26. Khan, S. A.; Khan, S. B.; Asiri, A. M., Layered double hydroxide of Cd-Al/C for the Mineralization and De-coloration of Dyes in Solar and Visible Light Exposure. *Scientific Reports* **2016,** 6, 35107.
27. Malak-Polaczyk, A.; Vix-Guterl, C.; Frackowiak, E., Carbon/Layered Double Hydroxide (LDH) Composites for Supercapacitor Application. *Energy & Fuels* **2010,** 24, (6), 3346-3351.
28. Daud, M.; Kamal, M. S.; Shehzad, F.; Al-Harthi, M. A., Graphene/layered double hydroxides nanocomposites: A review of recent progress in synthesis and applications. *Carbon* **2016,** 104, 241-252.
29. Zhao, M.-Q.; Zhang, Q.; Huang, J.-Q.; Wei, F., Hierarchical Nanocomposites Derived from Nanocarbons and Layered Double Hydroxides - Properties, Synthesis, and Applications. *Advanced Functional Materials* **2012,** 22, (4), 675-694.
30. Tichit, D.; Coq, B., Catalysis by Hydrotalcites and Related Materials. *CATTECH* 7, (6), 206-217.
31. Wang, J.; Mei, X.; Huang, L.; Zheng, Q.; Qiao, Y.; Zang, K.; Mao, S.; Yang, R.; Zhang, Z.; Gao, Y.; Guo, Z.; Huang, Z.; Wang, Q., Synthesis of layered double hydroxides/graphene oxide nanocomposite as a novel high-temperature CO_2 adsorbent. *Journal of Energy Chemistry* **2015,** 24, (2), 127-137.
32. Iruretagoyena, D.; Shaffer, M. P.; Chadwick, D., Adsorption of carbon dioxide on graphene oxide supported layered double oxides. *Adsorption* **2013**, 1-10.
33. Abelló, S.; Medina, F.; Tichit, D.; Pérez-Ramírez, J.; Rodríguez, X.; Sueiras, J. E.; Salagre, P.; Cesteros, Y., Study of alkaline-doping agents on the performance of reconstructed Mg–Al hydrotalcites in aldol condensations. *Applied Catalysis A: General* **2005,** 281, (1–2), 191-198.
34. Meis, N. N. A. H.; Bitter, J. H.; de Jong, K. P., On the Influence and Role of Alkali Metals on Supported and Unsupported Activated Hydrotalcites for CO_2 Sorption. *Industrial & Engineering Chemistry Research* **2010,** 49, (17), 8086-8093.
35. Tung, V. C.; Chen, L.-M.; Allen, M. J.; Wassei, J. K.; Nelson, K.; Kaner, R. B.; Yang, Y., Low-Temperature Solution Processing of Graphene−Carbon Nanotube Hybrid Materials for High-Performance Transparent Conductors. *Nano Letters* **2009,** 9, (5), 1949-1955.
36. Kong, H. X., Hybrids of carbon nanotubes and graphene/graphene oxide. *Current Opinion in Solid State and Materials Science*, (0).
37. Kim, K. H.; Oh, Y.; Islam, M. F., Graphene coating makes carbon nanotube aerogels superelastic and resistant to fatigue. *Nat Nano* **2012,** 7, (9), 562-566.
38. Peng, L.; Feng, Y.; Lv, P.; Lei, D.; Shen, Y.; Li, Y.; Feng, W., Transparent, Conductive, and Flexible Multiwalled Carbon Nanotube/Graphene Hybrid Electrodes with Two Three-Dimensional Microstructures. *The Journal of Physical Chemistry C* **2012,** 116, (8), 4970-4978.
39. Wang, Y.; Wu, Y.; Huang, Y.; Zhang, F.; Yang, X.; Ma, Y.; Chen, Y., Preventing Graphene Sheets from Restacking for High-Capacitance Performance. *The Journal of Physical Chemistry C* **2011,** 115, (46), 23192-23197.
40. Aboutalebi, S. H.; Chidembo, A. T.; Salari, M.; Konstantinov, K.; Wexler, D.; Liu, H. K.; Dou, S. X., Comparison of GO, GO/MWCNTs composite and MWCNTs as potential electrode materials for supercapacitors. *Energy & Environmental Science* **2011,** 4, (5), 1855-1865.
41. Dong, X.; Ma, Y.; Zhu, G.; Huang, Y.; Wang, J.; Chan-Park, M. B.; Wang, L.; Huang, W.; Chen, P., Synthesis of graphene-carbon nanotube hybrid foam and its use as a novel three-dimensional electrode for electrochemical sensing. *Journal of Materials Chemistry* **2012,** 22, (33), 17044-17048.
42. Tian, L.; Meziani, M. J.; Lu, F.; Kong, C. Y.; Cao, L.; Thorne, T. J.; Sun, Y.-P., Graphene Oxides for Homogeneous Dispersion of Carbon Nanotubes. *ACS Applied Materials & Interfaces* **2010,** 2, (11), 3217-3222.
43. Zhang, C.; Ren, L.; Wang, X.; Liu, T., Graphene Oxide-Assisted Dispersion of Pristine Multiwalled Carbon Nanotubes in Aqueous Media. *The Journal of Physical Chemistry C* **2010,** 114, (26), 11435-11440.

598 44. Zhu, X.; Tang, C.; Wang, H.-F.; Zhang, Q.; Yang, C.; Wei, F., Dual-sized NiFe layered double hydroxides in
599 situ grown on oxygen-decorated self-dispersal nanocarbon as enhanced water oxidation catalysts. *Journal of*
600 *Materials Chemistry A* **2015,** 3, (48), 24540-24546.
601 45. Rezaei, B.; Khosropour, H.; Ensafi, A. A.; Dinari, M.; Nabiyan, A., A new electrochemical sensor for the
602 simultaneous determination of guanine and adenine: using a NiAl-layered double hydroxide/graphene oxide-
603 multi wall carbon nanotube modified glassy carbon electrode. *RSC Advances* **2015,** 5, (92), 75756-75765.
604 46. Rodriguez-Pastor, I.; Ramos-Fernandez, G.; Varela-Rizo, H.; Terrones, M.; Martin-Gullon, I., Towards the
605 understanding of the graphene oxide structure: How to control the formation of humic- and fulvic-like oxidized
606 debris. *Carbon* **2015,** 84, 299-309.
607 47. Verdejo, R.; Lamoriniere, S.; Cottam, B.; Bismarck, A.; Shaffer, M., Removal of oxidation debris from
608 multi-walled carbon nanotubes. *Chemical Communications* **2007,** 0, (5), 513-515.
609 48. Rourke, J. P.; Pandey, P. A.; Moore, J. J.; Bates, M.; Kinloch, I. A.; Young, R. J.; Wilson, N. R., The Real
610 Graphene Oxide Revealed: Stripping the Oxidative Debris from the Graphene-like Sheets. *Angewandte Chemie*
611 *International Edition* **2011,** 50, (14), 3173-3177.
612 49. Patterson, A. L., The Scherrer Formula for X-Ray Particle Size Determination. *Physical Review* **1939,** 56,
613 (10), 978-982.
614 50. Qiu, L.; Yang, X.; Gou, X.; Yang, W.; Ma, Z.-F.; Wallace, G. G.; Li, D., Dispersing Carbon Nanotubes with
615 Graphene Oxide in Water and Synergistic Effects between Graphene Derivatives. *Chemistry – A European Journal*
616 **2010,** 16, (35), 10653-10658.
617 51. Moon, G. D.; Joo, J. B.; Yin, Y., Stacked multilayers of alternating reduced graphene oxide and carbon
618 nanotubes for planar supercapacitors. *Nanoscale* **2013,** 5, (23), 11577-11581.
619 52. Wang, H.; Kakade, B. A.; Tamaki, T.; Yamaguchi, T., Synthesis of 3D graphite oxide-exfoliated carbon
620 nanotube carbon composite and its application as catalyst support for fuel cells. *Journal of Power Sources* **2014,**
621 260, 338-348.
622 53. Gao, Y.; Zhang, Z.; Wu, J.; Yi, X.; Zheng, A.; Umar, A.; O'Hare, D.; Wang, Q., Comprehensive investigation
623 of CO_2 adsorption on Mg-Al-CO_3 LDH-derived mixed metal oxides. *Journal of Materials Chemistry A* **2013,** 1, (41),
624 12782-12790.
625 54. Sharma, U.; Tyagi, B.; Jasra, R. V., Synthesis and Characterization of Mg–Al–CO_3 Layered Double
626 Hydroxide for CO_2 Adsorption. *Industrial & Engineering Chemistry Research* **2008,** 47, (23), 9588-9595.
627 55. Cinke, M.; Li, J.; Bauschlicher Jr, C. W.; Ricca, A.; Meyyappan, M., CO_2 adsorption in single-walled carbon
628 nanotubes. *Chemical Physics Letters* **2003,** 376, (5–6), 761-766.
629 56. Ding, Y.; Alpay, E., High Temperature Recovery of CO_2 from Flue Gases Using Hydrotalcite Adsorbent.
630 *Process Safety and Environmental Protection* **2001,** 79, (1), 45-51.
631 57. Abellan, G.; Latorre-Sanchez, M.; Fornes, V.; Ribera, A.; Garcia, H., Graphene as a carbon source effects
632 the nanometallurgy of nickel in Ni,Mn layered double hydroxide-graphene oxide composites. *Chemical*
633 *Communications* **2012,** 48, (93), 11416-11418.
634 58. Matsukata, M.; Fujikawa, T.; Kikuchi, E.; Morita, Y., Interaction between potassium carbonate and
635 carbon substrate at subgasification temperatures. Migration of potassium into the carbon matrix. *Energy & Fuels*
636 **1988,** 2, (6), 750-756.
637 59. Menzel, R.; Iruretagoyena, D.; Wang, Y.; Bawaked, S. M.; Mokhtar, M.; Al-Thabaiti, S. A.; Basahel, S. N.;
638 Shaffer, M. S. P., Graphene oxide/mixed metal oxide hybrid materials for enhanced adsorption desulfurization of
639 liquid hydrocarbon fuels. *Fuel* **2016,** 181, 531-536.
640 60. Elyassi, B.; Wahedi, Y. A.; Rajabbeigi, N.; Kumar, P.; Jeong, J. S.; Zhang, X.; Kumar, P.; Balasubramanian,
641 V. V.; Katsiotis, M. S.; Andre Mkhoyan, K.; Boukos, N.; Hashimi, S. A.; Tsapatsis, M., A high-performance
642 adsorbent for hydrogen sulfide removal. *Microporous and Mesoporous Materials* **2014,** 190, 152-155.
643 61. Joshi, R. K.; Schneider, J. J., Assembly of one dimensional inorganic nanostructures into functional 2D
644 and 3D architectures. Synthesis, arrangement and functionality. *Chemical Society Reviews* **2012,** 41, (15), 5285-
645 5312.

646 62. Xia, Y.; Yang, P.; Sun, Y.; Wu, Y.; Mayers, B.; Gates, B.; Yin, Y.; Kim, F.; Yan, H., One-Dimensional
647 Nanostructures: Synthesis, Characterization, and Applications. *Advanced Materials* **2003,** 15, (5), 353-389.
648 63. Bai, S.; Xiong, Y., Recent Advances in Two-Dimensional Nanostructures for Catalysis Applications. *Science*
649 *of Advanced Materials* **2015,** 7, (10), 2168-2181.

650